Flight Physics Analysis for the FSTB-L Supersonic Business Jet

Falk Sachs*, Carsten Christmann†, Samuel Schnell‡, Daniel Kiehn§, Robin Hähnel¶
German Aerospace Center (DLR), Braunschweig, 38108, Germany

The project STORMIE (Supersonic Transport Open Research Models and Impact on Environment) addresses new concepts for supersonic passenger transport with special focus on low boom capabilities. For this purpose, three aircraft designs are set up and investigated. The first configuration, the Future Supersonic Transport Business Jet – Low Boom (FSTB-L), is a business jet designed to offer special low boom capabilities for $Ma = 1.4$. The second design envisages a supersonic airliner (FSTA) with a design cruise Mach number of $Ma = 1.7$ and the third design is a supersonic business jet (FSTB-N) designed for the same TLARs (top level aircraft requirements) as the FSTB-L but without special low boom design for benchmarking purposes. Several disciplines are brought together to converge to a consistent preliminary design. This paper reflects the flight mechanical investigations, their outcomes and influence on design, and the redesign of the aircraft to solve trim and stability issues. Special interest of this paper is on the first of three designs: a supersonic business jet (FSTB-L) in a canard configuration. Results of flight performance calculations, aerodynamic analyses and takeoff considerations are presented. This paper highlights fields of special interest within the flight mechanical analysis activities performed, which were major drivers in design process iteration loops. Those are investigations on the flight performance in cruise, the low speed characteristics of the aircraft concerning stability and a short analysis on the impacts of configuration changes for the takeoff.

I. Nomenclature

C_L	=	Lift coefficient
$C_{m,Can}$	=	Pitching moment coefficient due to canard deflection
$C_{m,\eta}$	=	Pitching moment coefficient due to elevator deflection
c_p	=	Pressure coefficient
D	=	Drag
F	=	Force
$F_{Z,MLG}$	=	Z-force at main landing gear
$F_{Z,NLG}$	=	Z-force at nose landing gear
g	=	gravitational acceleration
L	=	Lift
l_T	=	Thrust lever arm w.r.t. the center of gravity
l_μ	=	Mean aerodynamic chord
m	=	Aircraft mass
Ma	=	Mach number
M_{Can}	=	Canard pitching moment
M_η	=	Elevator pitching moment
L	=	Lift
S_{ref}	=	Reference area
T_{total}	=	Total thrust
V_R	=	Rotation speed

*Research Aerospace Engineer, Institute of Flight Systems
†Research Aerospace Engineer, Institute of Flight Systems, AIAA Senior Member
‡Research Aerospace Engineer, Institute of Aerodynamics and Flow Technology
§Research Aerospace Engineer, Institute of Flight Systems
¶Research Aerospace Engineer, Institute of Flight Systems

V_{zrc}	=	Speed with zero rate of climb
V_{TAS}	=	True airspeed
V_2	=	Takeoff safety speed
$x_{MLG,CG}$	=	x-lever arm main landing gear w.r.t. the center of gravity
$z_{MLG,CG}$	=	z-lever arm main landing gear w.r.t. the center of gravity
$z_{T,CG}$	=	z-lever arm thrust force w.r.t. the center of gravity
γ	=	Flight path angle
μ_R	=	Friction coefficient
ρ	=	Density
σ_1	=	1st tipback control angle
σ_2	=	2nd tipback control angle
τ	=	Tail-down angle
χ	=	Azimuth angle

II. Motivation

Supersonic commercial flights have been executed over decades. The only long-term operated civil aircraft in this segment has been the Concorde. The last flight of the Concorde fleet ended in 2003 after 27 years of airline service. Since the Concorde development program ended considerations of environmental impact and technical burdens as well as the immense development costs for a supersonic aircraft program hindered further developments of comparable supersonic passenger aircraft.

Nowadays, new players are entering the market (Boom, Aerion). Enablers of the new technologies are more fuel-efficient turbo machines, new materials, and the advanced research on low boom technologies. Apart from the emissions perspective, noise is a driver of environmental impact with growing relevance and also financial impact [1].

Low boom concepts as proposed by NASA [2] are under investigation to overcome the issue of a loud supersonic boom to open the possibility for supersonic flights over land without excessive sound exposure on the ground. Such development would multiply the use cases for supersonic flights substantially.

The German Aerospace Center (DLR) has set up the project Supersonic Transport Open Research Models and Impact on Environment (STORMIE) to deliver profound aircraft designs for future supersonic aircraft and to share the outcomes with the scientific community and authorities to evaluate the impact of such aircraft on today's air traffic. A secondary objective is the classification of such aircraft for current and future regulations in close cooperation with NASA, JAXA, FAA, and EASA.

This paper focuses on the flight mechanics investigations of the FSTB-L configuration (Future Supersonic Transport Business Jet – Low Boom) shown in Fig. 1. The conceptual design is done with the preliminary aircraft design tool openAD [3] and the calculations for low and high fidelity aerodynamic data are done with LIFTING_LINE (low fidelity) and TAU (high fidelity), respectively. To check the design and the flight performance and dynamic behavior of the aircraft, flight mechanic investigations have to be executed. Those primarily cover stability and control as well as flight performance. The results are fed back in the design process and a close inter-domain exchange has been established to achieve a converged design, i.e. fulfilling all requirements including flyability. The software tools involved in these investigations exchange information via CPACS (Common Parametric Aircraft Configuration Schema) [4] which provides a common data exchange format based on an XML (Extensible Markup Language) data structure. This enables the different disciplines and tools to directly exchange and build upon each other's results, which is enhancing the design process.

III. Aircraft Simulation Framework

For the evaluation of the aircraft's flight dynamics, the 6-degrees-of-freedom (6DoF) fixed-wing aircraft simulation tool COAST (CPACS-Oriented Aircraft Simulation Tool) [5] was used. It is a MATLAB®/Simulink® implemented flight simulation specifically tailored to the structure of CPACS and was designed for the usage in MDO (multi-disciplinary optimization) toolchains. COAST consists of three main parts: CPACS import functions (so-called *wrapper functions*), a Simulink® simulation model, and postprocessing analysis code.

The implemented wrapper functions import relevant aircraft data from CPACS: they parse and import XML data to MATLAB® from the corresponding data structures (e.g., propulsion, aerodynamics) and restructure it to the format required by the simulation model. Internally, the wrapper functions rely on the MATLAB® interfaces of the open-source

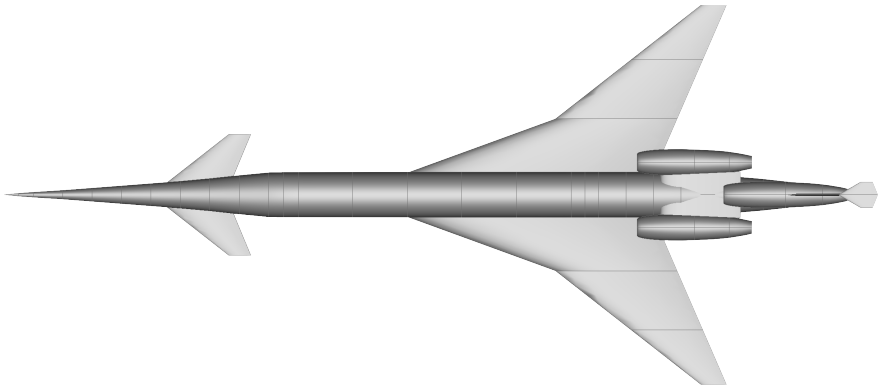

Fig. 1 FSTB-L (Future Supersonic Transport Business Jet – Low Boom)

libraries TiXI [6] and TiGL [7].

The simulation model is implemented in Simulink®; its structure is shown in Fig. 2. The non-CPACS specific components of the model (e.g., the equations of motion, Earth model, atmospheric model) are pure Simulink® implementations, and most CPACS-specific components (control chain, aerodynamics, propulsion) are implemented as C++ S-functions for better flexibility and processing speed. Within the STORMIE project COAST has been extended by a CPACS-specific landing gear model [8], which enables investigations of the takeoff and landing phases of the supersonic configuration including performance and noise assessments.

The COAST model includes a flight control system (FCS) based on a nonlinear model following control architecture and an integrated control allocation algorithm [5], which allows closed-loop simulation for a large variety of aircraft. The control allocation algorithm automatically determines the optimal* set of control surface deflections based on the effectiveness of the individual control surfaces at the given flight point: the user only needs to specify which control surfaces are available to the control allocator (e.g., to account for failed actuators) [5]. The FCS includes a normal law similar to those used in Airbus aircraft as well as a trajectory controller (in an outer loop), which causes the aircraft to follow given flight path angle γ and flight path azimuth angle χ.

The third component of COAST are (post-)processing functions for trimming, linearization, and analysis of stability and control characteristics. Additionally, COAST provides output interfaces to flight mechanics analysis tools, e.g., for flight performance evaluation (MAPET-FLT, cf. Section IV) or handling qualities analysis (HAREM [9, 10]).

Thanks to its high degree of flexibility, COAST has been used with a wide range of aircraft configurations such as unmanned combat air vehicles [11], fighter aircraft [12], supersonic civil aircraft such as the FSTB-L configuration investigated in this paper, and a hybrid-electric regional aircraft with Distributed Electric propulsion (DEP). The latter was flight tested in simulation using the interface between COAST and DLR's full flight simulator AVES[13, 14].

IV. In-Flight Performance Evaluation

The flight performance was evaluated using the software tool MAPET-FLT (Model-based Aircraft Performance Evaluation Tool - In-flight Performance), which was developed within a MATLAB® environment. The current version is an evolution of the tool described in Ref. [15]. The further development of this flight performance evaluation tool was mainly driven by the increased demand to analyze CPACS-based generic aircraft models in addition to aircraft-specific flight dynamics models, causing the need to adapt MAPET-FLT to the aircraft simulation framework COAST. The upgraded version of MAPET-FLT is the result of this development process, also incorporating major improvements and modifications compared to its predecessor. The objective of this section is to give an overview of the flight performance of the FSTB-L aircraft as part of the multi-disciplinary aircraft design process chain. The main purpose of the presented flight performance evaluation is to provide first insights into the flight mechanics of the low-boom supersonic aircraft concept.

*In the sense of the minimum two-norm.

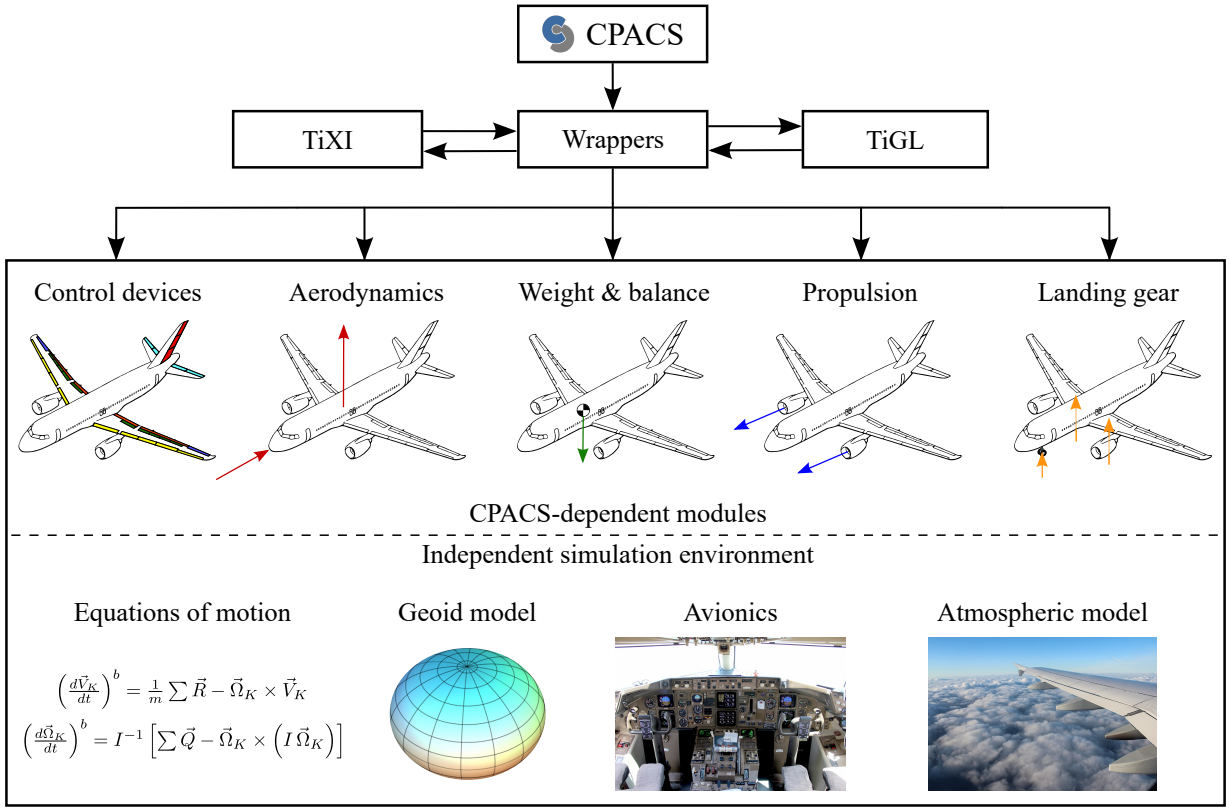

Fig. 2 COAST framework structure

A. Framework of Flight Performance Evaluation

The flight performance analysis within MAPET-FLT is divided into three main parts. The initial part is the preprocessing, followed by the solver and the postprocessing part. The core of the analysis process within MAPET-FLT is the solver part. The concept of determining aircraft flight performance is based essentially on trim calculations of different steady flight conditions. The trim calculations are performed by a trim routine that allows trimming aircraft states and control inputs. In the MAPET-FLT analysis flight conditions are called trim cases and can be characterized as steady cruise or steady thrust setting, respectively. For the steady cruise condition the aircraft is trimmed for unaccelerated horizontal level flight, and the power setting to maintain a flight path angle $\gamma = 0°$ is obtained automatically by the trim function at the given flight conditions. In the steady thrust condition, the trim problem is solved without using varying the engine thrust to obtain a force equilibrium: instead, the thrust is fixed at a pre-selected power setting. Depending on this power setting, the resulting flight path angle γ is somewhere between the steepest angle of descent (at minimum thrust) and the maximum achievable climb angle (or lowest angle of descent, if the engine thrust is insufficient for climb). For every trim case the total mass as well as altitude and Mach number are varied and the aircraft model is trimmed during the solving process yielding a unique trim point. The variation of these three dimensions within each trim case leads to a trim matrix for every trim case. The results for all trim points are stored for the subsequent postprocessing analysis in which the flight performance parameters are determined.

B. Estimation of the Flight Envelope

The estimation of the flight envelope is based on the evaluation of the trimmed aircraft at steady cruise conditions at discrete trim points. The trim routine calculates the thrust, the angle of attack and the control inputs to fulfill the steady cruise trim requirements for each discrete trim point (combination of fixed total mass, altitude, and Mach number). Consequently, the range of each trim matrix dimension should cover the estimated limits of the aircraft regarding its targeted flight performance.

In [16] concepts for landing and takeoff (LTO) noise and CO_2 emission requirements for supersonic transport (SST)

Table 1 Trim matrix range for flight performance evaluation

	Lower limit	Upper limit
Total aircraft mass	28,545 kg	42,680 kg
Altitude	0 m	16,000 m
Mach number	0.2	1.6

airplanes are described. The document also includes the definition of reference masses for specific air range (SAR) measurements. To account for the differences between subsonic airplanes and SST airplanes, a different approach is proposed instead. In this approach, high and low gross masses, representative of initial cruise and end-of-cruise conditions, are selected based on the airplane's design mission. For the FSTB-L, a high gross mass of 90 % MTOM (42,680 kg) and a low gross mass of 60 % MTOM (28,545 kg) were selected and used for the estimation of the flight envelope. The limits chosen for this analysis are given in Table 1. Figure 3 shows the trim results for steady cruise conditions.

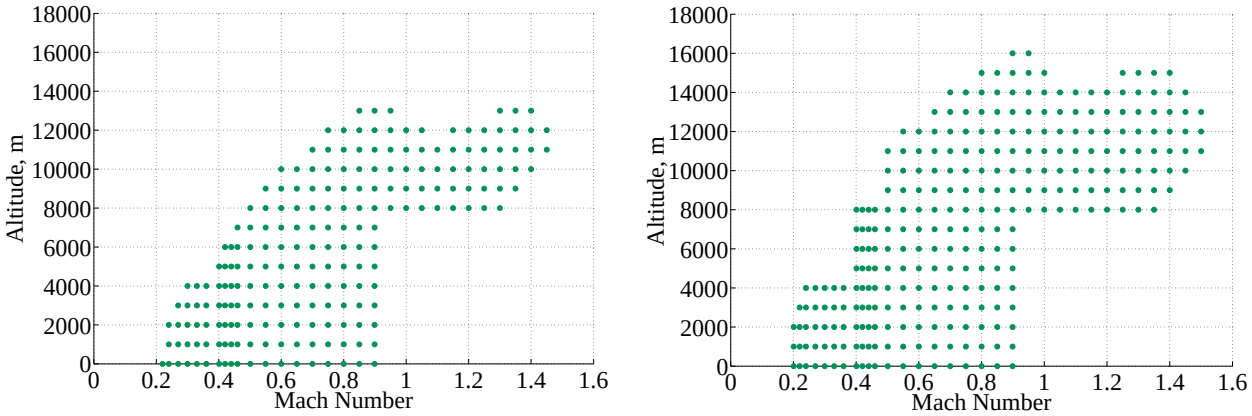

(a) High gross mass (90 % MTOM) **(b) Low gross mass (60 % MTOM)**

Fig. 3 Estimated flight envelope for different aircraft masses

The gap at Mach numbers above 0.9 and altitudes below 8,000 m is caused by the lack of corresponding aerodynamic data in this region. The development of the aerodynamic performance map is well-described in [17], including the associated challenges and limitations. While it is expected that the aircraft is able to fly within this Mach number and altitude range, the trim function considers these trim conditions to be invalid due to the lack of aerodynamic data. The same applies to the small gaps in the low speed region. More aerodynamic data are needed in this area to fully determine the flight performance-driven speed limits.

The boundaries of the flight envelope at high speed and high altitude are not caused by a lack of aerodynamic data, but insufficient engine thrust. As can be seen in selected thrust curves for high gross mass shown in Fig. 4, the required thrust (blue curve) exceeds the available thrust (magenta curve) not only at the edges of the Mach number range. For better detection, the corresponding Mach number ranges are highlighted with a reddish area. Between 12000 m and 13000 m altitude, the required thrust is greater than the available thrust even in the intermediate Mach range. As a consequence, acceleration to supersonic Mach numbers can only be performed at flight altitudes below 12,000 m during the initial phase of the cruise flight (at high gross mass). In the further course of the supersonic cruise flight, the flight altitude can be increased up to 15,000 m. The kink in the available thrust curve at around $Ma = 1.4$ is due to the maximum permissible compressor temperature (T3) being reached.

Another important flight parameter is the angle of attack which is shown in Fig. 5. The curves are only shown where a valid trim solution could be obtained; they hence show interruptions at higher altitudes due to the thrust and due to aerodynamic data restrictions at lower altitudes as explained earlier. In the supersonic flight regime, the angle of attack is slightly above zero at typical cruising altitudes. At low cruising altitudes, the aircraft experiences a negative angle of attack, with the corresponding altitude band being larger for light aircraft configurations. However, for takeoff and landing a much higher angle of attack is needed.

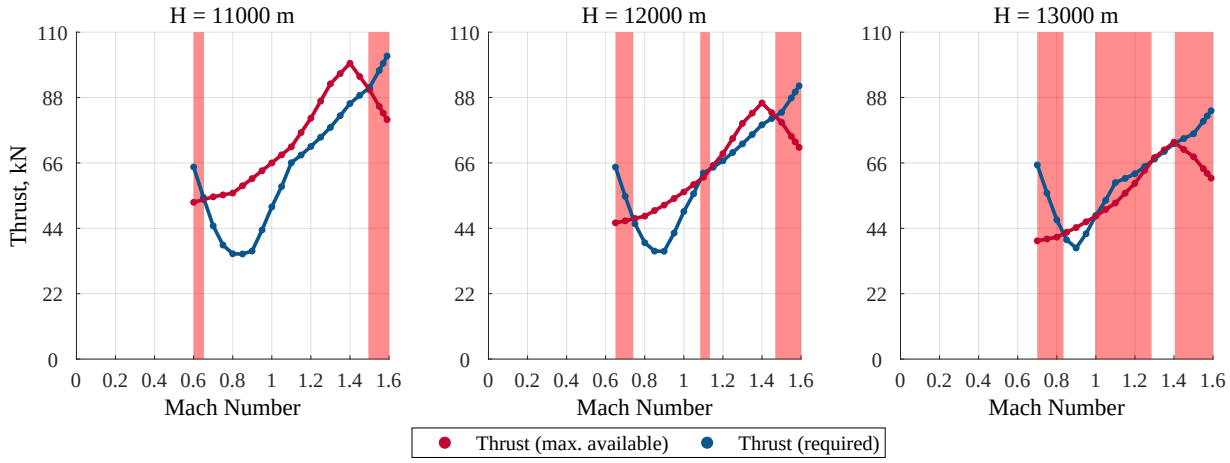

Fig. 4 Thrust curves for high gross mass (90 % MTOM)

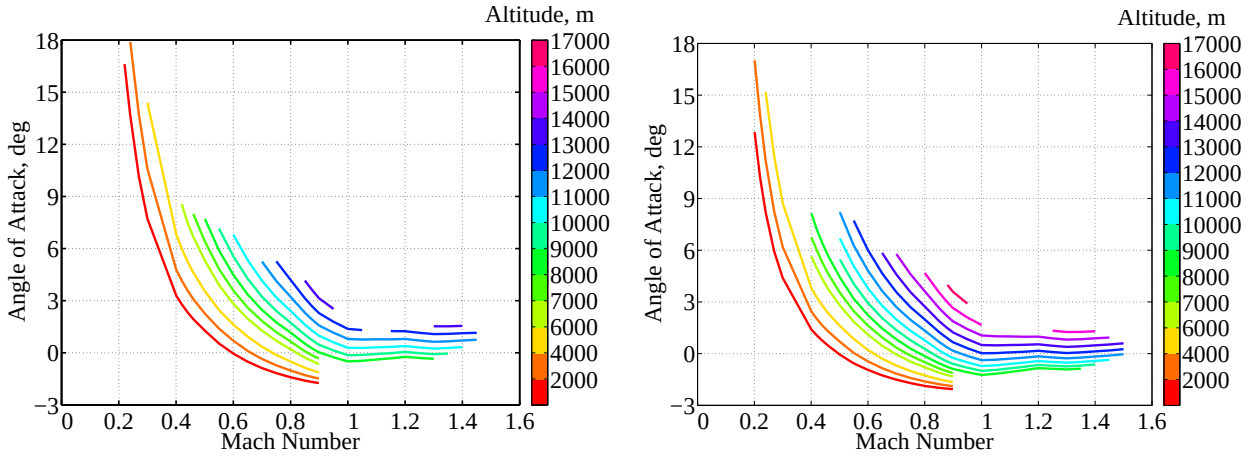

(a) High gross mass (90 % MTOM) **(b) Low gross mass (60 % MTOM)**

Fig. 5 Angle of attack curves for different aircraft masses at various altitudes

Figure 6 gives an impression of the stabilizer trim deflections at level flight conditions for two flight altitudes. Figure 6a shows two aircraft masses that are representative for takeoff (blue) and landing (red). During these flight phases, the center of gravity is in a forward position. It turns out that, particularly during takeoff with heavy aircraft, a significant amount of negative stabilizer deflection (trailing edge up, all notations follow [18]) is needed to trim the aircraft. It has to be noted, that in the takeoff and landing phase the center of gravity is assumed to be in forward position to increase static stability. In cruise flight condition, on the other hand, a rear center of gravity position is targeted. Figure 6b illustrates the stabilizer deflection curve at 12,000 m for both low and high gross mass. The stabilizer deflection is positive, but more than half of the available deflection is needed to trim the aircraft.

V. Low Speed Stability Characteristics

The FSTB-L's initial design is driven by two major concerns, namely the fuel efficiency and the noise. The environmental impact is a major concern to make supersonic commercial flights possible again. The general shape of the wing and the sizing of the aircraft are results of an openAD design process related to the top-level aircraft requirements (TLARs). The decision to use a canard as front stabilizer was driven by the intended low boom design: a canard providing nose-up trim changes the pressure signature of the sonic boom by distributing the lift along the longitudinal axis of the aircraft and leads to a more balanced pressure distribution as well as an arrangement of the supersonic shocks

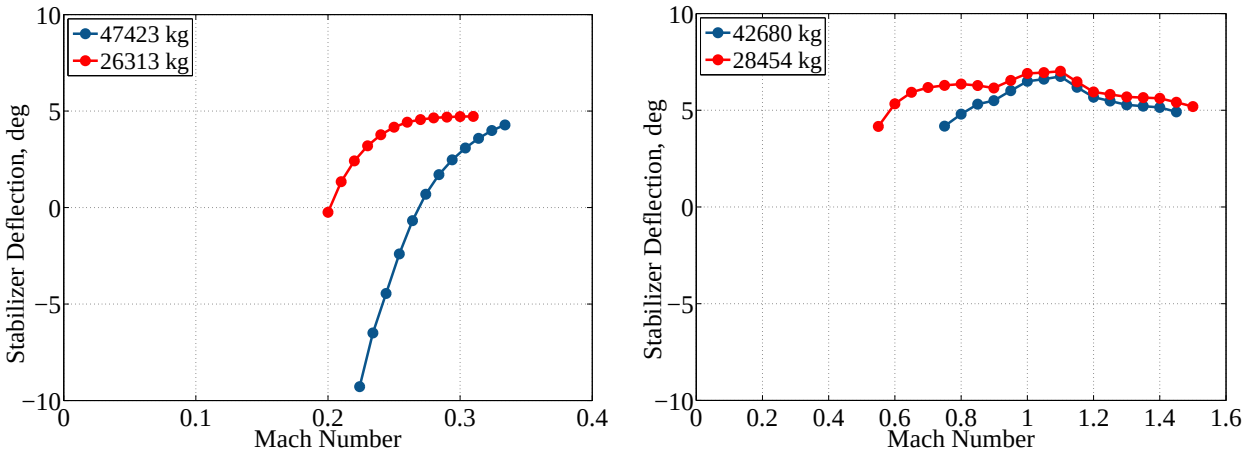

(a) Low altitude (0 m), forward cg

(b) High altitude (12,000 m), rear cg

Fig. 6 Stabilizer trim deflection at different altitudes

that is beneficial to reduce the supersonic boom [19]. However, adding a canard to the aircraft design imposes much more. The canard affects the geometry, positioning and sizing of the main wing, resulting in changes to the force and moment characteristics of the aircraft design. Especially the FSTB-L with its double-delta wing (cf. Figure 1) shows nonlinear effects in the pitching moment. Furthermore, the canard can affect the inflow of the main wing as well as the inflow of the engines at specific angles of attack. The canard is used for trim and control. In case of the present design those tasks are counteracting. The stabilizer needs to have sufficient surface to keep the aircraft trimmable, on the other hand a large surface of the canard in front of the center of gravity decreases the static stability of the aircraft. The wing shape and surface is designed for a maximum L/D in cruise flight, while maintaining sufficient maneuverability during takeoff and landing. Consequently, the wing has a high sweep and a low aspect ratio to keep the leading-edge of the wing inside the Mach cone.

In order to better assess the aircraft's maneuverability, especially the longitudinal stability during low speed flight like takeoff and landing, aerodynamic analyses are shown below using the present FSTB-L configuration. In Figure 7, the pitching moment coefficient is plotted against the angle of attack at $Ma = 0.3$ at sea level for the individual aircraft components. The data refer to the reference point of 27.64 m, which corresponds to the center of gravity with empty tanks (see Fig. 15). In addition, Figure 8 shows the corresponding pressure coefficient distributions for selected angles of attack. As expected, the canard has a positive slope in the pitching moment curve due to its position far in front of the reference point or center of gravity, which as a side effect also decreases the longitudinal static stability of the overall aircraft. The change in the pitching moment gradient is more critical for the design of the overall aircraft, as the configuration becomes more longitudinal statically unstable at angles of attack above 6°. As can be seen in Figure 7, the change is mainly due to the main wing. Comparing this with Fig. 8, one can see that the cause is the changing lift distribution in the longitudinal direction as the angle of attack increases. The lift is initially generated mainly in the outer part of the double delta wing. From an angle of attack of approx. 5-6°, the negative pressure area moves forward, starting from the main wing kink along the leading edge of the inner delta wing, which causes the change in the pitching moment gradient. The canard has a damping influence on the pitching moment gradient, as shown in [17] when comparing this configuration with and without canard. Overall, the influence of the canard on the pitching moment curve of the wing is relatively small, so that it can be neglected in the further course of this work.

Fig. 9 shows the influence of the canard for trimming and the corresponding trim margin. The yellow line describing the aircraft pitching moment with a canard deflection of 0° corresponds to the total aircraft pitching moment in Fig. 7. The other lines displayed in Fig. 9 show the moment coefficient of the aircraft with different canard deflections. The respective CG position is at 27.65 m. For all deflections a positive trend of c_m at angles of attack higher than 6° can be observed. It can also be seen, that the aircraft can be trimmed up to 16°. Nevertheless, the margin to pitch down the aircraft using the stabilizer alone decreases with increasing angles of attack, which is another consequence of the increase in c_m of the aircraft at angles of attack higher than 6°. While at an angle of attack of $\alpha = 5°$ the maximum pitching moment coefficient of $c_m = 0.07$ and a minimum of $c_m = -0.12$ can be reached at $\alpha = 16°$ the maximum is at $c_m = 0.11$ and the minimum at $c_m = 0.0$. That means with increasing angle of attack the canard is less effective and the

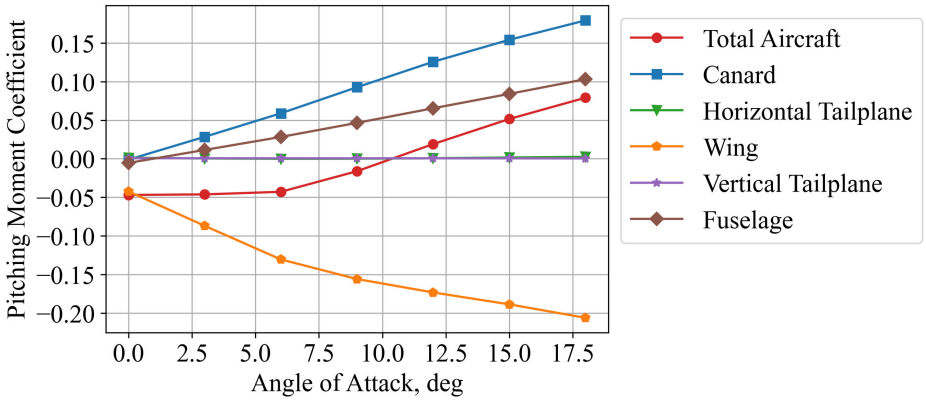

Fig. 7 Pitching moment coefficient per component at $Ma = 0.3$

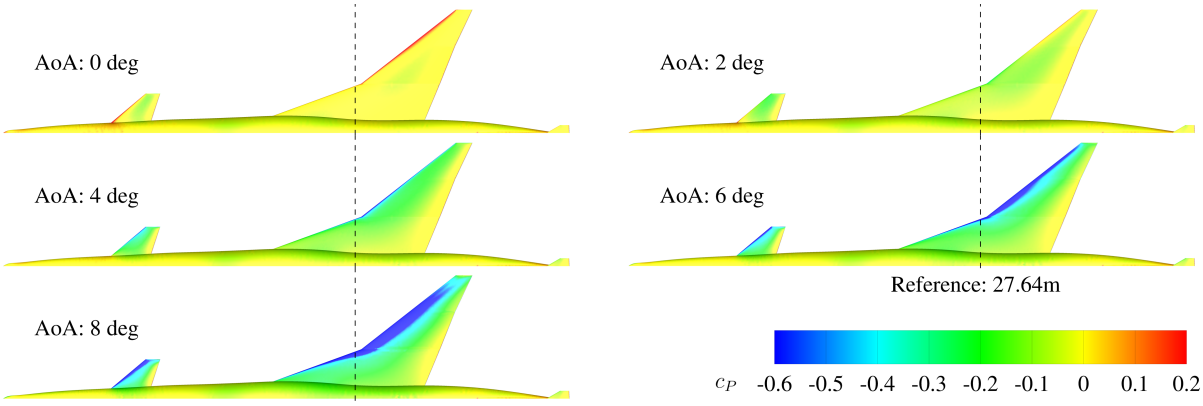

Fig. 8 Pressure coefficient variation for increasing angle of attack at low speed at $Ma = 0.3$

usability for active aircraft control is reduced drastically.

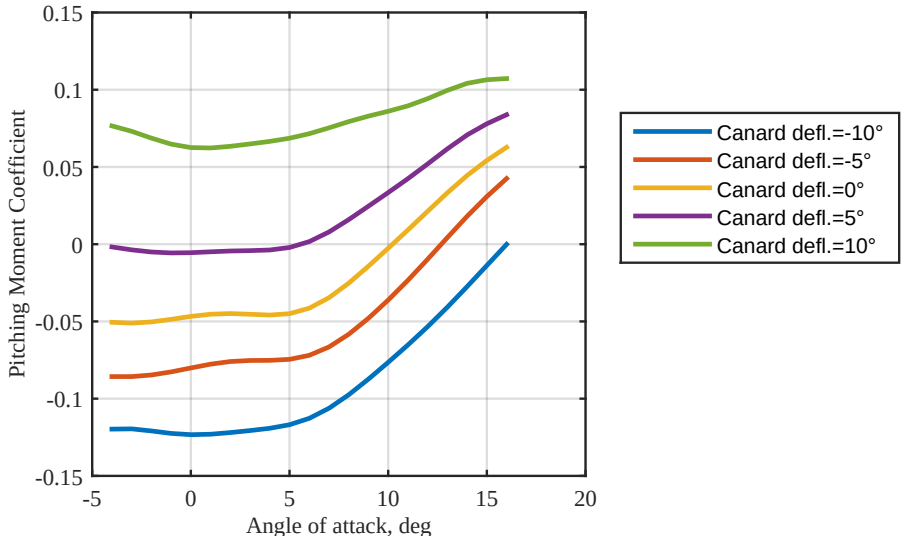

Fig. 9 Aircraft pitching moment at $Ma = 0.3$, altitude 0 m for different canard deflections

VI. Takeoff Performance of the FSTB-L

The reduction of noise emissions during supersonic cruise flight, such as those related to the supersonic boom, was the main driver for the FSTB-L design. But also noise related regulations for the lower airspace and low speed flight regimes have to be considered. Especially landing and takeoff has to be investigated for certification according to ICAO Annex 16, Vol I, Chapter 14 [20] noise standard for jet and propeller-driven airplanes. Such investigations have been started using the DLR tool FLIPNA (Flight Paths for Noise Analyses) [21]. FLIPNA is designed for point-wise calculation of the trajectory, which requires trimmed conditions to calculate each trajectory segment.

As the primary focus for the design of the aircraft is on the low noise aspects in cruise conditions, the takeoff performance is often a negatively impacted secondary factor. The sweep of the main wing is high to keep the leading edge within the Mach cone (roughly 46° at $Ma = 1.4$) at supersonic cruising speed, which leads to a low aspect ratio in combination with trailing edge flaps located far aft. Since those flaps have a large lever arm to the center of gravity, any positive deflection of the flaps to increase lift also produces a significant additional pitch down moment which has to be compensated by the canard or the elevators at the canard trailing edge. So even though a deflection of the flaps during takeoff would theoretically be beneficial in decreasing the required takeoff speed, this approach would compromise the control margin of the canard and the elevators due to their additional deflection. Consequently the controllability of the aircraft at low speeds would be negatively affected, making the procedure potentially infeasible. Instead other methods to improve takeoff performance have to be evaluated.

A. Engine Installation

The engine position of the design used in STORMIE has been chosen to enable an efficient shielding for the fan noise. The outer engine inlets are above the wing structure (see Fig. 1) which inhibits the direct sound propagation to the area below the airplane. Shielding also applies to the inner engine which is shielded by the engine pylons of the outer engines. The remaining source of engine noise is jet noise in takeoff scenarios. For landing the jet noise is much lower and the shielding of the fan noise causes a huge reduction of overall aircraft noise.

A preliminary noise certification assessment was conducted by applying the process chain developed in [22] to the FSTB-L configuration. The results indicate that the aircraft noise limits defined in ICAO Annex 16, Volume I, Chapter 14, which is the current most stringent noise chapter (applicable for subsonic jet aeroplanes), cannot be met. The cumulative margin, which describes the margin to the sum of the noise levels at flyover point, sideline point and approach point, of the FSTB-L is 16.3 EPNdB, which corresponds to an overshoot of merely 0.7 EPNdB.

In contrast, the engine positions vertically above the center of gravity cause a distinct nose down pitching moment depending on the thrust level. Especially during the takeoff roll when high thrust is applied the thrust related pitch down moment is at a maximum. The primary means to compensate the pitch down moments are the elevators in positive deflection as well as a positive canard deflection. Such deflections increase the lift at the canards and help rotate the aircraft. On the other hand the increased canard downstream interacts with the main wing. At the inner part of the main wing the local lift coefficient is reduced resulting in a higher takeoff speed. The reduction of the lift at the inner part of the wing in combination with the low aspect ratio wing shape shifts the center of lift slightly to the rear of the main wing which also causes a slight pitch-down effect.

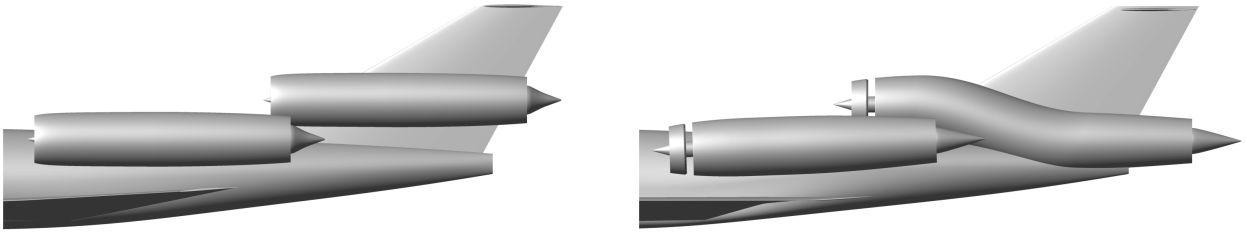

(a) Current tail design **(b) Enhanced tail design**

Fig. 10 Tailplane designs of the FSTB-L

To counteract the pitch-down effects of the engine as much as possible, the engine exhaust will be shifted downwards in the next design iteration. This becomes obvious regarding the S-shape of the middle engine (Fig. 10b) from inlet to

exhaust. In comparison to the original engine design, the pitch down moment portion will be reduced by up to 40 % by lowering the effective thrust lever arm l_T. Furthermore, the engines are tilted down by -2° to produce a downward thrust component. Those measures help reduce the thrust related pitching moment especially at takeoff.

Such an S-duct as shown in Fig. 10b also enlarges the effective surface of the vertical tailplane which is beneficial for lateral stability of the aircraft. In earlier designs, which were subject to prior investigations, the middle engine intersected the vertical tailplane and its airfoil (Fig. 10a).

B. Main Gear Position

The position of the landing gear has been determined according to [8] by analyzing the geometrical constraints posed for the landing gear and improving an initial positioning derived from the preliminary design produced with openAD. When deciding on the position of the main landing gear along the x-axis two control angles are most relevant, namely the tail-down angle and the tipback angle. The tipback angle is evaluated using two separate control angles illustrated in Fig. 11. The first one, here referred to as σ_1, is located between the static ground plane and a control plane, which is once again rotated along the y-axis until it intersects the fuselage but this time located in the contact point of the fully extended main gear. The second angle σ_2 is calculated by determining the angle of a line through the contact point of the statically loaded main gear and the center of gravity with the z-axis. When the aircraft is rotated about its y-axis, the projection of the center of gravity onto the ground plane can move behind the contact point of the main landing gear, causing the airplane to tip backward and remain tilted (referred to as a tipback).

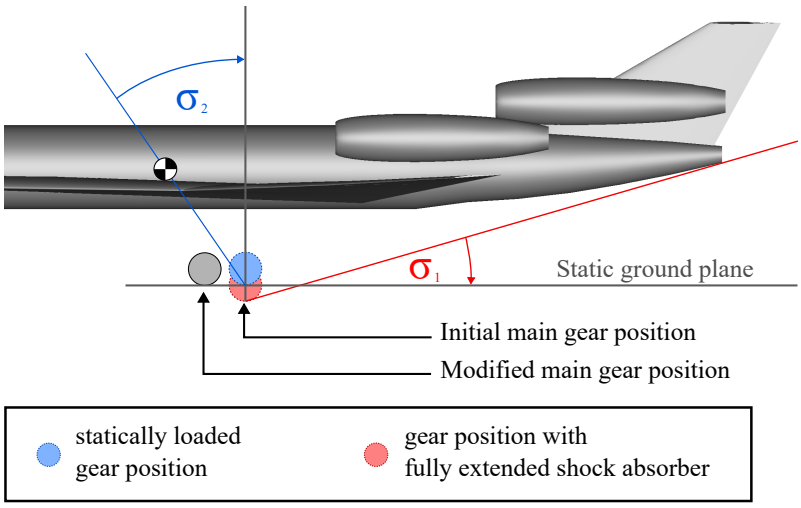

Fig. 11 Visualization of the tipback angle calculation with the initial and modified main gear positions

The tail-down angle (here referred to as τ) is used to assess the tailstrike condition. It is located between a horizontal plane through the contact point of the statically loaded main gear (static ground plane) and another plane placed at that same point but rotated around the y-axis until it intersects the fuselage structure. The effect of different main gear positions on all of these control angles is visualized in Fig. 12.

The following conditions are used to assess the adequacy of the chosen landing gear position [23].

- Condition 1: The tail-down angle τ is between 12° and 15°
- Condition 2: The angle σ_2 is greater than 15° (specifically highlighted in Fig. 12b)
- Condition 3: The angle σ_2 is greater than the angle σ_1

Both condition 1 and 2 are guideline estimates developed for traditional airliner configurations. As the FSTB-L utilizes a highly specialized configuration, the applicability of these conditions should be reviewed. Condition 3 however implies that a tipback should never occur during landing, as the fuselage will strike the ground before the center of gravity can move behind the contact point of the main gear. In general a more rearward position of the main landing gear reduces the risks of tailstrike and tipback of the airplane.

Next to these design considerations, it needs to be noted that a further rearward position is disadvantageous for takeoff performance: the longer the lever arm between the center of gravity and the main gear, the higher the aerodynamic moment required to rotate at takeoff. In this way, moving the main gear closer to the center of gravity will reduce the

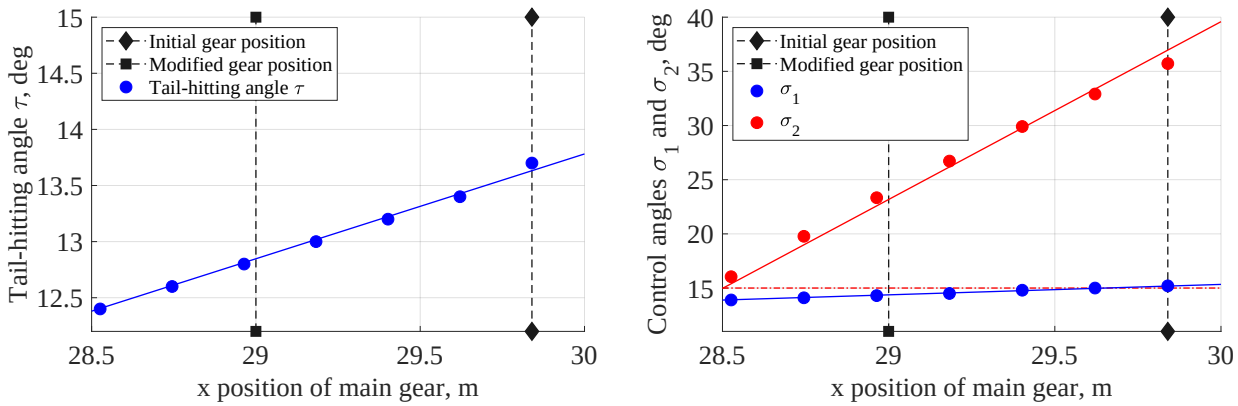

(a) Tail-down angle at varied main gear positions

(b) Tipback angle at varied main gear positions

Fig. 12 Landing gear design control angles at different x-positions of the main landing gear with the z-position left unchanged

effective lever arm of the weight force and reduce the takeoff distance. Exclusively modifying the horizontal position of the main gear would result in a decrease of the tail-down angle as shown in Fig. 12a. The FSTB-L is designed to land at high angles of attack as shown in Fig. 5, so such a change would complicate the landing of the aircraft. To offset the decrease in θ from moving the landing gear forward, a proposition is made to simultaneously increase the length of the landing gear. Different modifications to the main gear position in the x and z directions have been evaluated with respect to the aforementioned conditions, see Fig. 13.

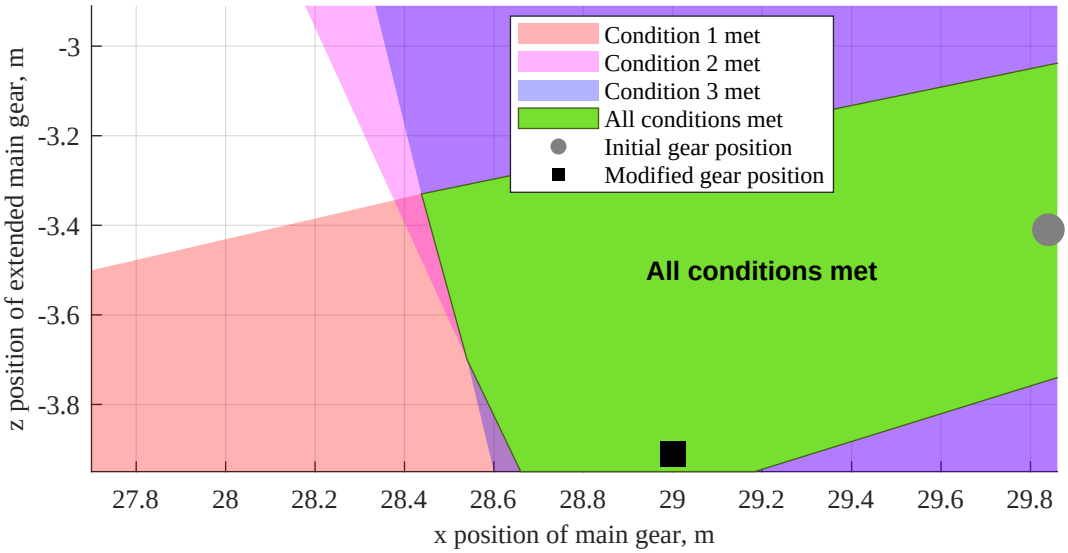

Fig. 13 Evaluation of different landing gear positions based on the design conditions

Figure 13 shows with which combinations of x and z positions of the main landing gear the individual conditions can be met and specifically highlights the positions which fulfill all three conditions. For optimal takeoff performance the revised position of the main gear should be as far forward as possible. The final position was chosen to stay firmly within the boundaries of the previously set conditions to minimize the risks of tailstrike and tipback. The result of these analyses yields a modified gear position (see Table 2) with a significantly shorter lever arm to the center of gravity and an increased tail-down angle.

Table 2 Initial and modified main gear positions with the corresponding tail-down and tipback conditions

	Gear contact point [x;y;z]	τ	σ_1	σ_2
Initial position	[29.84 m; ± 2.9 m; -3.41 m]	13.7°	15.2°	35.7°
Modified position	[29.00 m; ± 2.9 m; -3.91 m]	14.8°	16.3°	20.8°

C. Aerodynamic Surface Design

Since the wing design for the FSTB-L is mainly driven by high speed performance rather than takeoff performance [24] a comparably high takeoff roll speed has to be taken into account by nature. To reduce the takeoff roll and the speed at lift off, various design parameters have been adapted and will be investigated further. Key aspects are the wing installation angle of the main wing, which had been increased during the ongoing design loops, an adaption of the wing planform and a change of wing twist to counteract the inherent zero lift moment.

The main wing installation angle is designed appropriately for cruise flight at $Ma = 1.4$. At this Mach number the aircraft angle of attack is at 0.5° to 1.5° depending on flight altitude and overall weight. Since this correlates with the wing angle of attack to generate sufficient lift the installation angle is 0°. Due to the low aspect ratio of the wings, the contribution of the fuselage to overall lift for maximum glide ratio is higher compared to that of subsonic passenger aircraft. To generate this lift, the fuselage angle of attack needs to be positive. In [25] it is pointed out, that the fuselage contributes up to 11% to the overall lift for a cruise flight condition. Since the aspect ratio and the angle of attack of the current design are similarly high in cruise flight, one can assume a similar lift distribution for the present version of the FSTB-L. A comparison of different types of fuselages including a duck nose design has shown, that the influence of the nose design on the fuselage lift at cruise flight is less than $c_L \leq 0.001$ and therefore negligible for conceptual design.

An adaption of the horizontal stabilizer surface (canard or T-tail surface) is under investigation to increase static stability in low speed flight at takeoff or landing. In a future design step either the canard volume coefficient will be decreased and additional pitching moment created by the wing flaps or the T-tail horizontal surface will be enlarged to form a proper stabilizer surface while keeping the canard geometry as in the current design. The reasons for poor static stability are explained in section V. The decision to use a canard as a longitudinal control and stabilization surface is also driven by low noise aspects ([24], [26]) but clearly poses challenges to the overall aircraft design.

D. Center of Gravity Position in Takeoff

The FSTB-L configuration shows reduced static stability at low Mach numbers and high angles of attack. To keep the aircraft in stable conditions for as high angles of attack as possible, the center of gravity position should be maximum forward (section V). In contrast the capability of the aircraft to rotate is negatively affected by a forward position of the center of gravity. In this regard a more aft position would be favorable. The center of gravity can be shifted by pumping fuel into a designated trim tank. The Concorde had trim tanks installed in the front and the rear of the aircraft. The FSTB-L has a trim tank with a capacity of 2664 kg in the rear of the aircraft, directly behind the main gear bay (Fig. 14).

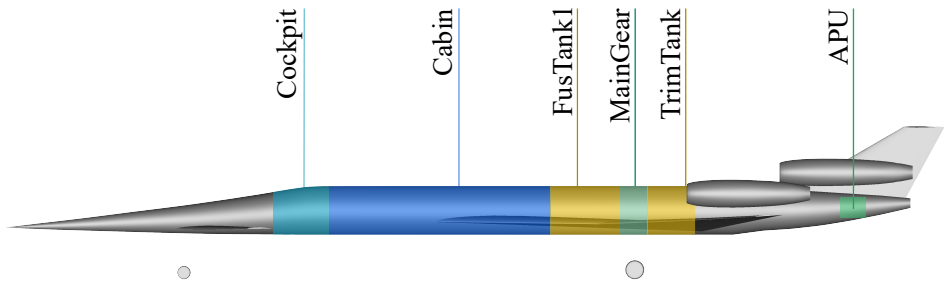

Fig. 14 Relevant mass fractions in the fuselage of FSTB-L

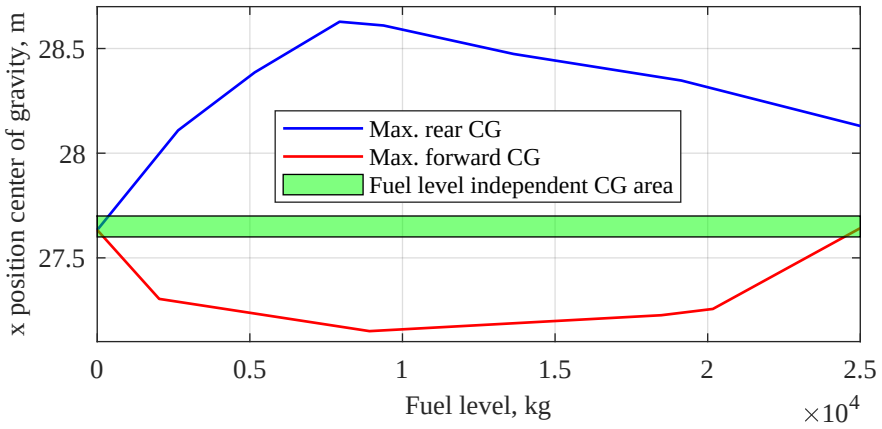

Fig. 15 Center of gravity position at different fuel levels

E. Takeoff Run Prediction

For the STORMIE project the estimation of sound emissions is crucial to determine the applicability of the configuration for future deployment. Especially if the aircraft is close to the ground the prediction of sound exposure values is of greatest interest. The jet noise of the supersonic cruise engines is higher than those of turbofan engines of current subsonic aircraft of comparable aircraft size with higher bypass ratio (the STORMIE bypass ratio is 2.3 - 3.1 depending on thrust condition). Furthermore the fan noise is different from known commercial aviation designs. Additionally a delta wing configuration with optimized wing surface for cruise conditions needs a comparably high ground roll speed at takeoff. As a consequence the thrust of the engines has to be sufficiently high to accelerate the aircraft on ground. To deal with all these effects the DLR tool FLIPNA is used to evaluate the sound immissions on the ground. FLIPNA calculates a trajectory based on simple assumptions for ground roll distance and calculates trim conditions for each flight point after lift-off. The flight paths are obtained by stringing together individual operating points of the trimmed aircraft without taking into account the dynamic processes in between different operating points.

The trajectories calculated with FLIPNA may be compared with those generated using COAST (Fig. 16). COAST is capable of reflecting dynamic behavior and transitions, which is not possible using FLIPNA. Consequently the flight trajectory can be determined with COAST in a more realistic way. Comparing the results of FLIPNA and COAST helps to verify the FLIPNA results. An important example is the takeoff procedure. The takeoff run has to be investigated independently from previous analysis. Transferring the knowledge of the borders of the flight envelope on the takeoff procedure may be misleading since the ability of the control surfaces to produce a certain aerodynamic force changes radically according to the angle of attack. So in a possible example it may be, that the stall speed is lower than the speed needed to rotate on the runway.

To evaluate the impact of design factors as explained in previous sections, various simulations may be performed or even more simple considerations can be used. Figure 17 shows the predominant forces in takeoff.

During the takeoff run the lift L and the drag D are increasing with airspeed. The angle of attack of the FSTB-L is roughly 0°. The effective thrust lever arm to the center of gravity is negative and in combination with the thrust of all three engines T_{total} it causes a pitch down moment. The drag nearly causes no pitch moment around the center of gravity since its force application point is close to it. And finally the landing gear is also producing a moment as the respective z- and x-forces have a lever arm to the center of gravity. Three simple equations for the sum of x-forces, z-forces and the pitching moment can be set up. The special condition for the moment the aircraft starts to rotate is, that the force $F_{z,NLG}$ is eliminated. Adding this condition to the equations paves the way to reformulate the equations to calculate the airspeed V_R at which the aircraft may start to rotate as shown in equation 1.

$$V_R = \sqrt{\frac{-T_{total} \cdot z_{T,CG} - m \cdot g \cdot (x_{MLG,CG} - \mu_R \cdot z_{MLG,CG})}{\rho/2 \cdot S_{ref} \cdot (C_L \, (-x_{MLG,CG} + \mu_R \cdot z_{MLG,CG} + x_{NP,CG}\,) + (C_{m,Can} + C_{m,\eta}\,) \cdot l_\mu)}} \tag{1}$$

Equation 1 contains a dependency on the total thrust of the aircraft T_{total}, which itself is a function of the airspeed,

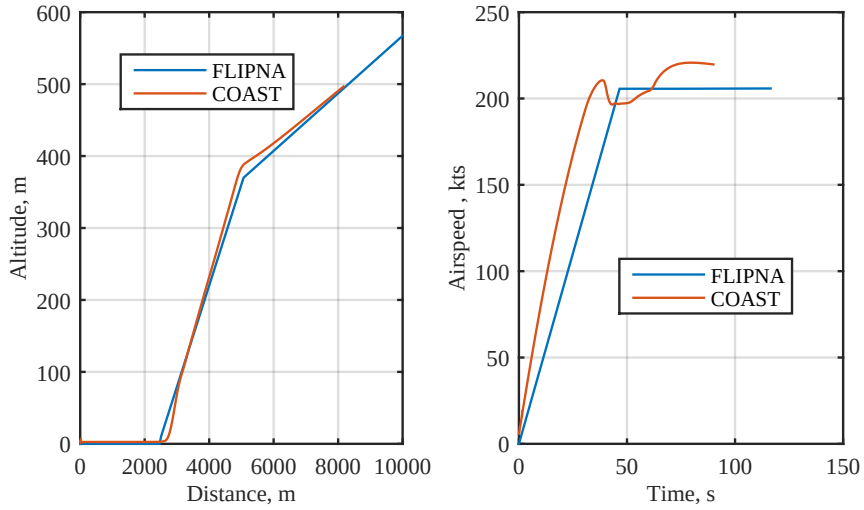

Fig. 16 Verification of FLIPNA predicted trajectories by COAST (example using low fidelity aerodynamic data)

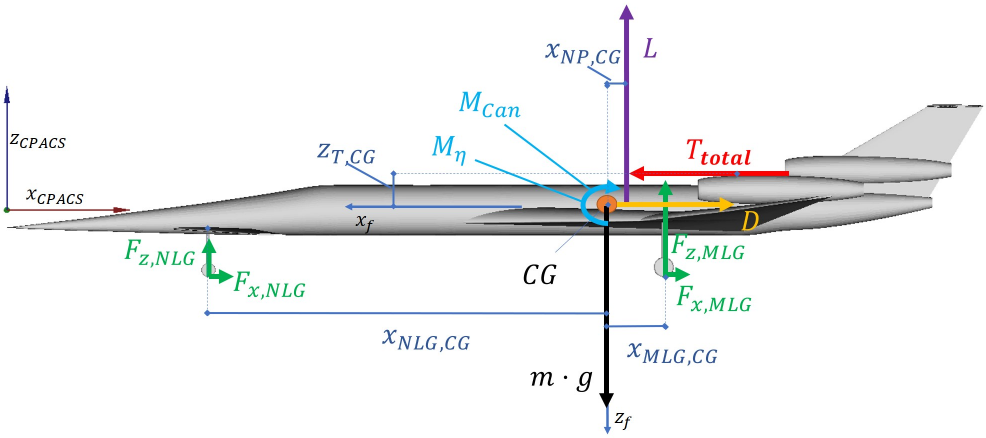

Fig. 17 FSTB-L: forces, moments and lever arms in takeoff

altitude and thrust lever position. For simplification the according values are taken from the engine performance tables at an altitude of 0 m MSL in standard atmosphere and the thrust lever command is at the maximum possible value for takeoff (derated). To solve this issue of interdependency equation either Eq. 1 may be solved iteratively or Eq. 1 may be computed for a huge set of possible values for T_{total} and the set of results checked for the correct pairing of V_{TAS} and T_{total} from Fig. 18 to find the correct result.

Using COAST an acceleration run on the ground with maximum thrust applied up to 250 kts has been simulated to calculate the required runway length and takeoff time corresponding to V_R. From those results the values for takeoff acceleration time t_R (Fig. 19 lower right graph) until V_R (Fig. 19 upper left graph) and the passed runway distance x_R are derived to be shown in Fig. 19 and Fig. 20

Fig. 19 presents the impact of an adaption of the engine positions relative to the initial FSTB-L configuration. The lever arm of the thrust line of the total thrust (3 engines) may be reduced from 1.2 m to 0.75 m by the measures presented in Figure 10b. Such reduction of the thrust line lever arm $l_{T,CG}$ reduces the rotation speed by 6 kts and the roll distance by about 100 m. It is clearly beneficial for takeoff to reduce the impact of the thrust related pitch down moment. Moreover, the reduction of this moment also helps reduce trim drag during cruise flight and increases the overall aircraft performance accordingly.

In a second parameter study the x-position of the main landing gear (MLG) is changed. The impact on the minimum

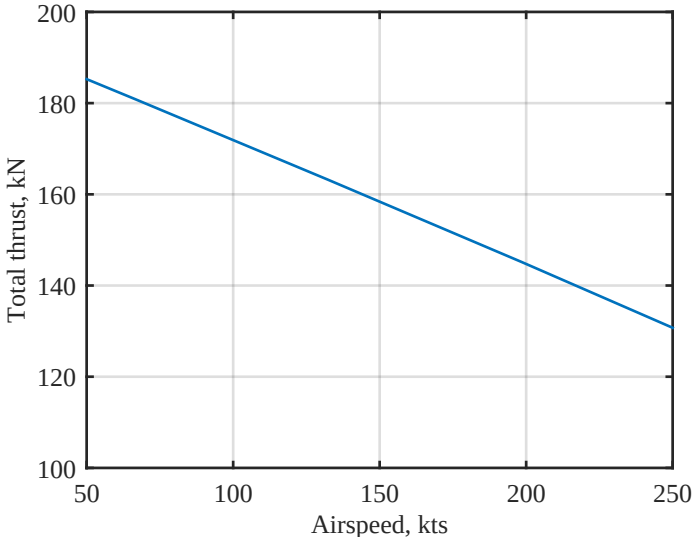

Fig. 18 FSTB-L total available thrust depending on airspeed at mean sea level

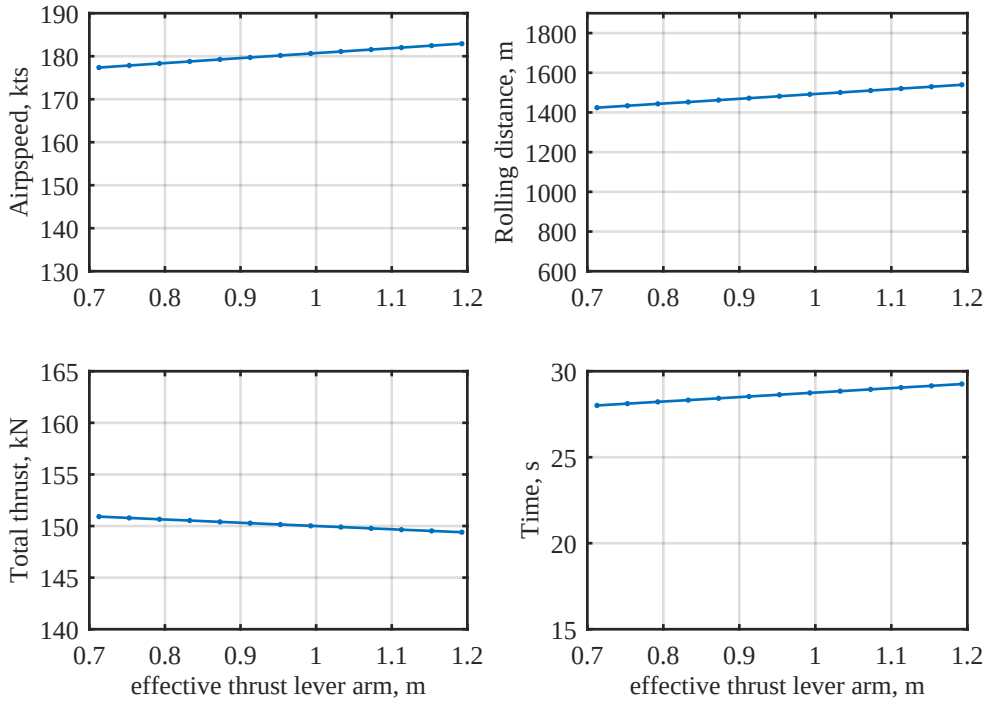

Fig. 19 Takeoff performance parameters for variation of thrust lever arm

rotation speed V_R is more significant. The baseline aircraft for these trials is the FSTB-L configuration with the adapted engine position, shown in Fig. 10b, and also used in the previous calculation (compare Fig. 19). Fig. 20 displays the effect of moving the main gear position forward. By reducing the lever arm $x_{MLG,CG}$ the moment of the vertical force $F_{Z,MLG}$ around the CG is reduced. By shifting the MLG position forward by 1 m, still respecting the geometrical constraints described in Fig. 13, a V_R of 132 kts can be achieved.

This configurational change reduces the achievable minimum takeoff roll distance from 1450 m to 700 m, a reduction

of more than 50 %. The lower left plot shows the remaining thrust at the moment of rotation. The lower the speed of rotation, the higher the remaining thrust according to Fig. 18.

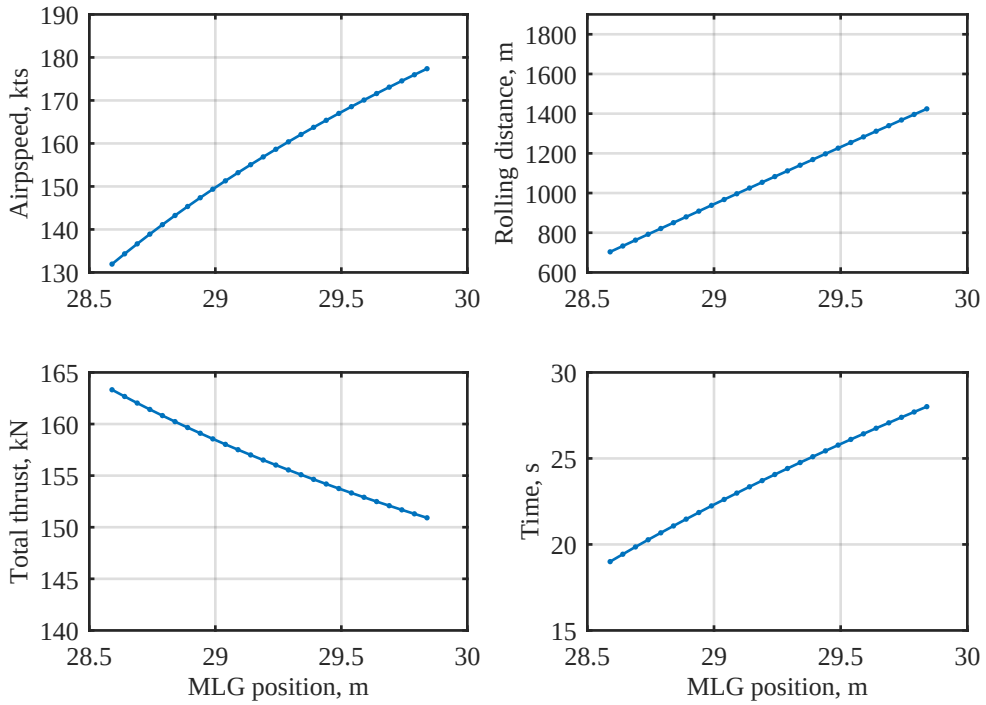

Fig. 20 Takeoff performance parameters for variation of main landing gear (MLG) x-position

The investigations shown in Fig. 19 and Fig. 20 reveal which speeds are necessary for aircraft rotation during the takeoff run when applying the proposed design changes to the main gear position and the engine installation setup. In all cases shown the canard as well as the elevators are deflected to their maximum extent to deliver an aerodynamic force sufficient to rotate the aircraft. For the following initial climb and climb-out phases however further boundaries have to be taken into account.

The delta-wing configuration has some unique characteristics when compared to a more conventional configuration. One characteristic is that delta-winged aircraft do not stall in the usual manner [27]. At the same time, important speeds relevant to the certification of takeoff and landing are dependent on stall characteristics. Consequently, for the certification of the Concorde a parameter V_{zrc} was introduced for the takeoff procedure [27]; it denotes the speed at which the rate of climb reaches zero when on three engines (i.e., one engine inoperative). Even if a rotation of the

Table 3 Airspeeds at selected altitudes and maximum takeoff mass with a zero rate of climb (one engine inoperative case)

	0 m	500 m	1000 m	1500 m	2000 m
True airspeed, kts	169.3	180.2	192.3	204.2	218.5
Angle of attack, deg	13.26	12.05	10.89	9.95	8.90
Thrust, kN	102.1	94.2	86.5	79.4	72.3
Stabilizer deflection, deg	-2.02	-0.33	1.09	2.03	2.96

FSTB-L aircraft at the lowest speed shown in Fig. 20 (132 kts) is achievable by changes to the design, it is not reasonable to pursue such a radical change of the main gear position. Table 3 displays characteristic values for the flight at V_{zrc} the airspeed at which the maximum rate of climb is limited to zero with one engine inoperative. Losing one engine while airborne at a speed below V_{zrc} could be catastrophic for the aircraft. In such a situation the aircraft has to accelerate

to reduce its drag. Since the remaining engines are already working at maximum possible thrust, the only solution is to descend and gain speed, which is not possible if close to the ground. Nonetheless it is rational to apply design changes to reach a theoretical rotation speed of, e.g., 150 kts with full elevator and canard deflection. In a practical takeoff scenario the canard will be deflected to a much lower extent and the pitch control column/stick does not have to be pulled as far. In that case the aircraft will rotate at a higher speed than shown in Fig. 20. Especially a lower canard deflection is favorable for takeoff since it has to be moved quickly to its trim position for initial climb as shown in Table 4 for climb angles of $\gamma = 10°$. It may be assured by cockpit procedures to ensure that the climb out will be performed at sufficiently high flight speeds. Table 4 shows results from trim calculations for climb outs with climb

Table 4 Thrust requirements at selected airspeeds and maximum takeoff mass with a 10° flight path angle

	170 kts	175 kts	180 kts	185 kts	190 kts	195 kts	200 kts	205 kts	210 kts
Flight path angle, deg	10.00	10.00	10.00	10.00	10.00	10.00	10.00	10.00	10.00
Thrust, kN	130.6	128.2	126.1	124.1	122.4	120.9	119.4	118.1	117.0
Angle of attack, deg	12.84	12.12	11.45	10.82	10.24	9.69	9.18	8.70	8.25
Stabilizer deflection, deg	9.58	9.06	8.60	8.20	7.84	7.52	7.24	6.98	6.75

angles $\gamma = 10°$. According to the calculated values the three engines offer sufficient thrust to perform 10° climbouts at the speeds given and at MTOM of 47.5 t.

VII. Conclusions

The project STORMIE aims to deliver three supersonic aircraft configurations, which will be made publicly available. This paper focuses on the research activities in the field of flight physics on the FSTB-L, a supersonic business jet with low boom characteristics. The framework for flight mechanic simulations based on CPACS aircraft data is introduced and results for from trim calculations are shown. The presented data gives an impression of the flight envelope and shows several borders of the flight envelope, which are explained in more detail. It turned out, that the aircraft in its current design is capable to fly up to 16000 m and can reach a maximum Mach number of 1.5 at an altitude of 12000 m. Furthermore the implications of the chosen configuration for static stability are presented and the corresponding behavior of the aircraft explained with data from high fidelity aerodynamic calculations. Those considerations give insights in the aerodynamic processes that lead to a significant shift of the aerodynamic center in low speed, which affects static stability in low speed flight. Additionally, as a distinct example for interdisciplinary design and collaboration the determination of the takeoff rotation speed is presented. The outcomes of these rather simple flight mechanical studies are fed back into the simulation environment and the same environment will then be used to validate the results of noise calculations during takeoff.

References

[1] Flughafen Berlin Brandenburg GmbH, "Charges Regulation Berlin Brandenburg Airport (Valid from 2024-01-01)," https://corporate.berlin-airport.de/content/dam/corporate/de/geschaeftspartner/entgelte/entgeltordnung-ber.pdf, 2023. Accessed: 16th May 2025.

[2] Doebler, W. J., Wilson, S. R., Loubeau, A., and Sparrow, V. W., "Simulation and Regression Modeling of NASA's X-59 Low-Boom Carpets Across America," *Journal of Aircraft*, Vol. 60, No. 2, 2023, pp. 509–520. https://doi.org/10.2514/1.C036876.

[3] Wöhler, S., Atanasov, G., Silberhorn, D., Fröhler, B., and Zill, T., "Preliminary Aircraft Design within a Multidisciplinary and Multifidelity Design Environment," *Aerospace Europe Conference 2020*, Council of European Aerospace Societies, 2020.

[4] Alder, M., Moerland, E., Jepsen, J., and Nagel, B., "Recent Advances in Establishing a Common Language for Aircraft Design with CPACS," *Aerospace Europe Conference 2020*, Council of European Aerospace Societies, 2020.

[5] Kiehn, D., Autenrieb, J., and Fezans, N., "COAST - A Simulation and Control Framework to Support Multidisciplinary Optimization and Aircraft Design with CPACS," *33rd Congress of the International Council of the Aeronautical Sciences*, International Council of the Aeronautical Sciences (ICAS), 2022.

[6] DLR e.V. (German Aerospace Center), "GitHub - DLR-SC/tixi: A simple XML interface library," https://github.com/DLR-SC/tixi, 2025. Accessed: 16th May 2025.

[7] DLR e.V. (German Aerospace Center), "The TiGL Geometry Library," https://dlr-sc.github.io/tigl, 2025. Accessed: 16th May 2025.

[8] Hähnel, R., "Modellbildung, Implementierung und Simulation eines parametrisierbaren Fahrwerkmodells für ein Überschallverkehrsflugzeug," Masterarbeit, TH Wildau, 2024. URL https://elib.dlr.de/208031/.

[9] Ehlers, J., "Flying Qualities Analysis of CPACS Based Aircraft Models – HAREM V2.0," Tech. Rep. DLR-IB 111-2013/21, DLR Institute of Flight Systems, 6 2013. URL https://elib.dlr.de/83046/.

[10] Hasan, Y. J., Flink, J., Freund, S., Klimmek, T., Kuchar, R., Liersch, C. M., Looye, G., Moerland, E., Pfeiffer, T., Schrader, M., and Zenkner, S., "Stability and Control Investigations in Early Stages of Aircraft Design," *2018 Applied Aerodynamics Conference*, 2018. https://doi.org/10.2514/6.2018-2996.

[11] Kiehn, D., Diekmann, J. H., and Fezans, N., "Design and Multi-Objective Optimization of a Control Surface Allocation Concept for an Agile and Highly Swept Flying Wing," *Deutscher Luft- und Raumfahrtkongress*, 2018. URL https://elib.dlr.de/125264/.

[12] Christmann, C., Kiehn, D., Stradtner, M., and Liersch, C. M., "Initial Assessment of Stability and Controllability in the Early Stage of Combat Aircraft Design," , 2023. https://doi.org/10.25967/570283.

[13] Duda, H., Advani, S. K., and Potter, M., "Design of the DLR AVES Research Flight Simulator," *AIAA Modeling and Simulation Technologies (MST) Conference*, American Institute of Aeronautics and Astronautics, Reston, Virginia, 2013. https://doi.org/10.2514/6.2013-4737.

[14] Vechtel, D., and Buch, J.-P., "Aspects of yaw control design of an aircraft with distributed electric propulsion," *CEAS Aeronautical Journal*, Vol. 13, No. 4, 2022, pp. 847–860. https://doi.org/10.1007/s13272-022-00595-1.

[15] Ohme, P., and Raab, C., "A Model-Based Approach to Aircraft Performance Assessment," *AIAA Atmospheric Flight Mechanics Conference and Exhibit*, American Institute of Aeronautics and Astronautics, Reston, Virgina, 2008. https://doi.org/10.2514/6.2008-6873.

[16] European Union Aviation Safety Agency, "Environmental protection requirements for supersonic transport aeroplanes: A-NPA 2022-05," , 22 May 2022.

[17] Schnell, S., Tidow, A., and Kirz, J., "Multi-Fidelity Aerodynamic Data Set Generation and Analysis of the FSTB-L Supersonic Business Jet," *AIAA AVIATION 2025 Forum*, American Institute of Aeronautics and Astronautics, 2025.

[18] International Organization for Standardization, "Flight dynamics - Concepts, quantities and symbols: Part 1: Aircraft motion relative to the air," https://www.iso.org/standard/5699.html, 1989. ISO 1151-1:1988(en).

[19] Zhang, L., Han, Z., Qiao, J., Song, W., Ding, Y., and Wang, X., "Effect of longitudinal lift distribution on sonic boom of a canard-wing-stabilator-body configuration," *Chinese Journal of Aeronautics*, Vol. 36, No. 6, 2023, pp. 92–108. https://doi.org/10.1016/j.cja.2023.03.043.

[20] International Civil Aviation Organization, "Annex 16: Environmental Protection: Volume I — Aircraft Noise Eighth Edition, July 2017," , 2017.

[21] Blinstrub, J., "Immission-Based Noise Reduction within Conceptual Aircraft Design," Dissertation, Technische Universität, Braunschweig, 2019. https://doi.org/10.34912/fl8ght_n01s3.

[22] Nöding, M., Bertsch, L., Kirz, J., Ewert, R., and Berton, J. J., "Application and comparison of proposed SST noise certification regulations to a conceptual business aircraft," *AIAA AVIATION 2023 Forum*, American Institute of Aeronautics and Astronautics, Reston, Virginia, 2023. https://doi.org/10.2514/6.2023-4169.

[23] Currey, N. S., *Aircraft Landing Gear Design: Principles and Practices* , American Institute of Aeronautics & Astronautics, 1988. https://doi.org/10.2514/4.861468.

[24] Weber, L., Bertram, P., Dietl, T., Schnell, S., Plohr, M., and Liebhardt, B., "Conceptual Design of Supersonic Air Transport Configurations," *AIAA AVIATION 2025 Forum*, American Institute of Aeronautics and Astronautics, 2025.

[25] Schnell, S., "Development of an aerodynamic surrogate model for conceptual supersonic aircraft design based on DLR TAU simulations," *AIAA AVIATION Forum 2023*, 2023. https://doi.org/10.2514/6.2023-3726.

[26] Kirz, J., Schnell, S., Sachs, F., and Christmann, C., "CFD-based Design of a Supersonic Business Jet for Low Environmental Impacts Including Trim and Stability Constraints," *AIAA AVIATION 2025 Forum*, American Institute of Aeronautics and Astronautics, 2025.

[27] Eames, J. D., "Concorde Operations," *SAE Technical Paper Series*, SAE International, Warrendale, Pennsylvania, 1991. https://doi.org/10.4271/912161.